10-2017

Use of a Novel Infrared Wavelength-tunable Laser Mueller-matrix Polarimetric Scatterometer to Measure Nanostructured Optical Materials

Jason C. Vap

Stephen E. Nauyoks
Air Force Institute of Technology

Michael R. Benson

Michael A. Marciniak
Air Force Institute of Technology

Recommended Citation

J.C. Vap, S.E. Nauyoks, M.R. Benson, and M.A. Marciniak, Rev. Sci. Instrum. 88, 103104 (2017). https://doi.org/10.1063/1.4990003

Review of Scientific Instruments

Use of a novel infrared wavelength-tunable laser Mueller-matrix polarimetric scatterometer to measure nanostructured optical materials

Cite as: Rev. Sci. Instrum. **88**, 103104 (2017); https://doi.org/10.1063/1.4990003
Submitted: 13 June 2017 . Accepted: 21 September 2017 . Published Online: 10 October 2017

Jason C. Vap, Stephen E. Nauyoks, Michael R. Benson, and Michael A. Marciniak

Use of a novel infrared wavelength-tunable laser Mueller-matrix polarimetric scatterometer to measure nanostructured optical materials

Jason C. Vap,[1,2] Stephen E. Nauyoks,[3,4] Michael R. Benson,[3,5] and Michael A. Marciniak[3]
[1]*Department of Electrical and Computer Engineering, Air Force Institute of Technology, Wright-Patterson AFB, Ohio 45433, USA*
[2]*846 Test Squadron, Holloman AFB, New Mexico 88330, USA*
[3]*Department of Engineering Physics, Air Force Institute of Technology, Wright-Patterson AFB, Ohio 45433, USA*
[4]*Oak Ridge Institute of Science and Education, Belcamp, Maryland 21017, USA*
[5]*Materials and Manufacturing Directorate Air Force Research Laboratory, Wright-Patterson AFB, Ohio 45433, USA*

(Received 13 June 2017; accepted 21 September 2017; published online 10 October 2017)

Nanostructured optical materials, for example, metamaterials, have unique spectral, directional, and polarimetric properties. Samples designed and fabricated for infrared (IR) wavelengths have been characterized using broadband instruments to measure specular polarimetric transmittance or reflectance as in ellipsometry or integrated hemisphere transmittance or reflectance. We have developed a wavelength-tunable IR Mueller-matrix (Mm) polarimetric scatterometer which uses tunable external-cavity quantum-cascade lasers (EC-QCLs) to tune onto and off of the narrowband spectral resonances of nanostructured optical materials and performed full polarimeteric and directional evaluation to more fully characterize their behavior. Using a series of EC-QCLs, the instrument is tunable over 4.37-6.54 μm wavelengths in the mid-wave IR and 7.41-9.71 μm in the long-wave IR and makes measurements both at specular angles, acting as a Mm polarimeter, and at off-specular angles, acting as a Mm scatterometer. Example measurements of an IR thermal metamaterial are shown. *Published by AIP Publishing.* https://doi.org/10.1063/1.4990003

I. INTRODUCTION

Modern optical materials may be designed to have unique spectral, directional, and polarimetric optical properties. We have developed a unique, spectrally tunable, fully Stokes-polarimetric scatterometry system in the infrared (IR) specifically for the characterization of nanostructured optical materials, e.g., photonic crystals, plasmonic structures, and metamaterials.[1–4] Nanostructured IR materials offer unique measurement challenges. Theoretical predictions of optical metamaterials have shown that the effective material parameters of interest, electric permittivity (ε), and magnetic permeability (μ) will often depend on the incident angle and polarization of the incident radiation.[5,6] Also, the attribution of optical phenomena observed or predicted for these materials, e.g., to Bragg resonance as opposed to constitutive, homogeneous (effective) material parameters, based on inclusion size and periodicity, may not be clear cut.[7,8] Finally, these optical phenomena, often based on Bragg or plasmonic resonances, are typically narrow band in nature.[9,10] Past characterization of fabricated visible/IR optical nanostructured materials has included Fourier-transform-spectrometric specular transmittance,[11–14] reflectance,[15–17] and emittance,[18–26] IR spectraphotometric specular transmittance and reflectance,[27,28] IR prism-spectrometer emittance,[29,30] Variable-Angle Spectrometric Ellipsometry (VASE),[9] and hemispheric absorptance measured with an integrating sphere.[31,32] However, the capability to perform optical characterization of fabricated nanostructured material samples which is complete from a spectral, polarization, and directional point of view has not been available to IR nanostructured material researchers.

Narrowband performance features of nanostructured optical materials are often observed using a broadband instrument. A spectrometer typically provides the reflectance and transmittance data at normal incidence or fixed, specular reflectance or transmittance angles. When increasing the measurement space to include polarization-sensitive measurements, a VASE also provides the data at specular angles. Further, the IR-VASE typically provides a limited polarimetric evaluation, i.e., co- and cross-polarization [s-polarization incident/s-polarization reflected, pp, sp or ps] measurements and only partial Mueller-matrix (Mm) extractions. For fully polarimetric characterization at IR wavelengths both at and away from specular (and both in and out of the plane of incidence), an IR Mm polarimetric scatterometer is required. However, typical scatterometers are often limited in their ability to characterize nanostructured optical materials by their fixed-wavelength laser sources.

We have incorporated a series of IR-tunable external-cavity quantum-cascade lasers (EC-QCLs) to address this. Six tunable EC-QCLs (Daylight Solutions®) were selected to span a nearly continuous range of mid-wave IR (MWIR, 4.37-6.54-μm) and long-wave IR (LWIR, 7.41-9.71-μm) wavelengths and added to two fixed-wavelength 3.39-μm HeNe and 10.6-μm CO_2 lasers in a Schmitt Measurement Systems (SMS) Complete Angle Scatter Instrument (CASI®). Extensive hardware and software upgrades were also implemented to introduce an achromatic Dual Rotating Retarder (DRR) polarimeter with automated rotation stages associated with this instrument. The end product is a spectrally tunable IR Mm polarimetric scatterometer, which can be tuned into and out of narrowband performance regions of nanostructured optical materials,

allowing for the investigation of their full range of spectral, directional, and polarimetric behaviors.

II. INSTRUMENT

A. General scatterometer layout

CASI already had an existing and suitable beam train for the introduction of additional laser sources, but modifications were made so EC-QCLs could be introduced and easily aligned. Figure 1 shows turning mirrors (TMs) and a beam combiner (BC) to couple EC-QCLs into the beam path. As importantly, they also co-align a visible laser into the same beam path to facilitate the initial system alignment. Alignment is also facilitated by power adjustments to the EC-QCL, where a thermal paper is used to trace the IR beam through the system from the source to detector. Careful alignment is required to locate the IR beam on the front surface of the sample at the center of rotation of the goniometer (right side of Fig. 1, where the incident, θ_i, and scatter, θ_s, angles are measured from the sample normal). θ_i and θ_s are measured accurately only after this careful alignment.

B. Spectrally tunable IR sources

Six tunable EC-QCLs span much of the MWIR and LWIR wavelengths. Table I shows the tunable range of each EC-QCL, their peak wavelengths, and maximum powers. Unlike discharge lasers, the power of an EC-QCL is directly adjustable, which is effective for alignment, improvement of signal detection, and achieving the largest dynamic range possible for the instrument. The output powers of the 3.39-μm HeNe and 10.6-μm CO_2 lasers are 3.7 mW and 14.6 W, respectively.

The wavelength tuning ranges of the sources were tested using a 721B spectrum analyzer (Bristol Instruments®)

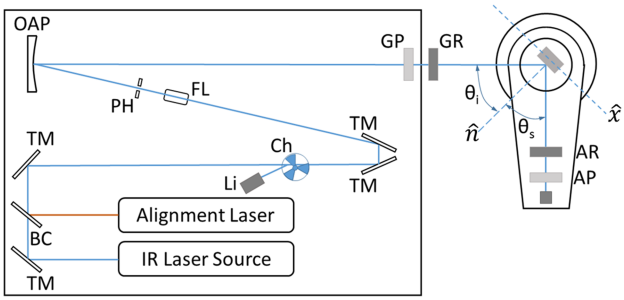

FIG. 1. Overhead-view schematic of the tunable Mm polarimetric scatterometer. IR-source and visible-alignment lasers are aligned along the optical path using turning mirrors (TMs) and a beam combiner (BC). The beam is chopped by a chopper (Ch) to allow lock-in detection with a lock-in amplifier (Li). The beam is focused through a pinhole (PH) by a focusing lens (FL), and the diverging beam is focused through the sample location onto the detector by an off-axis parabolic (OAP) mirror to provide nearly collimated incidence on the sample. The pinhole provides background suppression for the detector looking back at the source. The sample mount is on the right at the center of rotation of a goniometer; incident (θ_i) and scatter (θ_s) angles are measured from the sample normal ($\hat{n}$). The detector is at the end of the goniometer arm, which moves independently of sample position. The sample may also be tipped about its $\hat{x}$-axis for out-of-plane measurements. A Stokes polarization state is generated with a polarizer (GP)-retarder (GR) generator pair and analyzed with another retarder (AR)-polarizer (AP) analyzer pair.

TABLE I. EC-QCLs selected for the Mm polarimetric scatterometer.

EC-QCL wavelength range (μm)	λ_{peak} (μm)	Maximum power (mW)
4.35-4.55	4.5	220
4.74-5.15	4.9	160
5.16-5.67	5.3	330
5.76-6.54	6.1	280
7.40-8.23	7.8	340
8.06-9.71	8.8	

and found to have excellent wavelength stability with bias. The sample set of results shown in Table II demonstrates that the tuned-to-measured wavelength deviation is strongly correlated to the tuned wavelength rather than being dependent on the applied bias current. In general, the EC-QCL wavelength is able to be set to six significant-digit accuracy with a relative uncertainty of less than 0.2%, and laser line-widths are less than 30 MHz continuous wave and 30 GHz pulsed.

Automated wavelength tuning of the EC-QCLs is not currently the capability of our instrument. The scatterometer requires stringent alignment, however, the EC-QCLs wavelengths are tuned using a grating which creates enough beam walk that, when translated over the length of the optical path, necessitates manual readjustments in order to maintain alignment.

C. Achromatic polarimetric components

The most complex element of this instrument is the achromatic DRR polarimeter. A DRR polarimeter can determine the full Mm of a sample under test using a polarization state generator (GP and GR in Fig. 1) before the sample and polarization state analyzer (AR and AP in Fig. 1) after the sample, provided the retarders (GR and AR) are not half-wave plates ($\lambda/2$ retarders). The two retarders rotate at different rates, producing a data set of generated/analyzed polarizations from which the Mm may be extracted. Up-front analysis was conducted to determine the optimal retardance configuration and the best AR:GR rotation combination,[3,4,8] both of which leverage an existing calibration method.[33] Low-error Mm extractions are only possible with robust calibration methodology. We concluded that a (θ_A:θ_G = 5ω:1ω) Fourier rotation scheme,[34] where θ_A is the rotation increment of AR and θ_G is the rotation increment of GR, such that the AR angular rotation increments (ω) are five times larger than those of GR, was optimal by applying the condition number and error analysis.[4]

TABLE II. EC-QCL wavelength stability performance under different bias conditions.

EC-QCL tuned wavelength (μm)	Measured wavelength (μm)	Deviation (μm)
5.763 62 (at 500 mA)	5.751 13	0.012 49
5.843 00 (at 450 mA)	5.832 17	0.010 83
6.083 00 (at 400 mA)	6.076 69	0.006 31
6.535 86 (at 450 mA)	6.536 73	−0.000 87
6.535 86 (at 500 mA)	6.536 73	−0.000 87

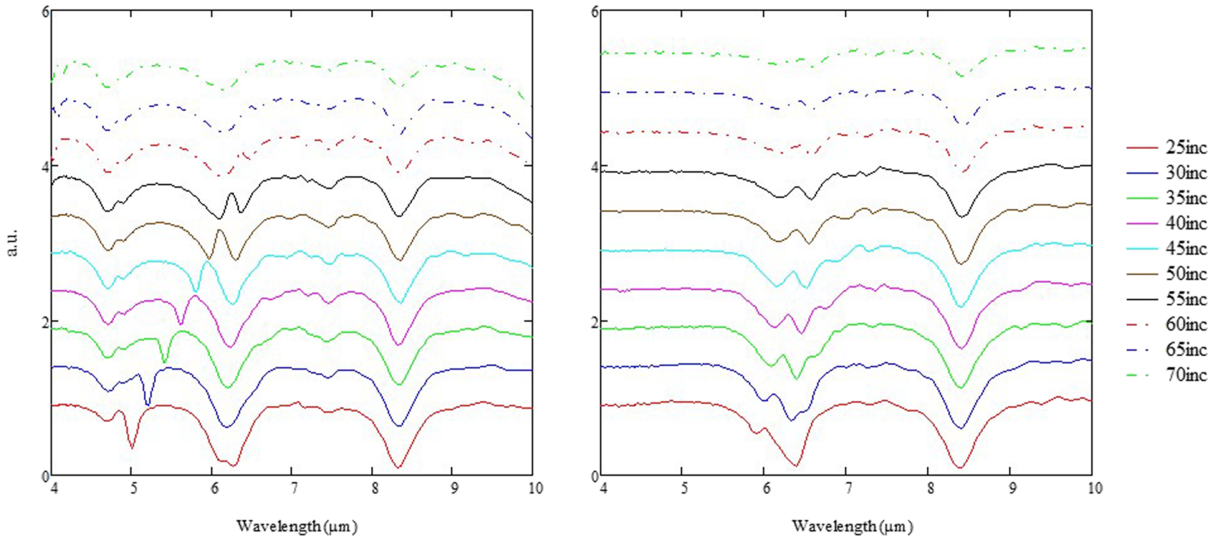

FIG. 2. P-pol (left) and s-pol (right) reflectance measurements of the MMA taken with the IR-VASE with increasing incident angles.

The traditional Fourier rotation scheme uses quarter-wave plates (λ/4 retarders), but we found that Chenault's calibration methodology[33] could also be used for our optimal λ/3 retardance configuration[35,36] and was better.[4]

Achromatic, nominally λ/3, CdS/CdSe wave-plates were obtained from Gooch and Housego LLC for both the MWIR and LWIR wavebands. Actual retardance values ranged 113°-127° and 109°-116° for the 4.3-6.5-μm and 7.4-10.6-μm bands, respectively. Four high-precision AGR-50 rotation stages (Aerotech, Inc.) were added and electronically integrated into CASI to achieve the DRR configuration. AGR-50 has an internal 50:1 angular reduction ratio giving a calculated, repeatable step size of 0.016° when driven by a 0.8° increment stepper motor.[1,2] This is well within the 0.3° DRR accuracy recommended by Goldstein.[37] Electronic drivers for the Aerotech stages of the DRR were installed and interfaced with the existing instrument software. Software modifications were made to produce a seamless transition from the typical scalar directional scans of the commercial CASI to our polarimetric scans.[1,2]

Using Fourier rotation schemes of (θ_A:θ_G = 25°:5°) and (37.5°:7.5°), free-space Mm extractions at less than 1% error are consistently achieved. An example free-space Mm extraction is

$$M_{free-space} = \begin{bmatrix} 1.0000 & 0.0010 & 0.0016 & -0.0019 \\ -0.0003 & 0.9978 & -0.0053 & 0.0012 \\ -0.0002 & 0.0065 & 0.9951 & 0.0010 \\ -0.0027 & -0.0016 & -0.0051 & 0.9969 \end{bmatrix}, \quad (1)$$

where the ideal free-space Mm is the identity matrix.

III. EXPERIMENTAL RESULTS AND ANALYSES

To illustrate the capabilities of our instrument, Mm results from a spectrally, directionally, and polarimetrically selective IR metamaterial absorber (MMA) sample, similar to that reported by Liu,[16] are shown in Secs. III A and III B with the instrument behaving first as a Mm polarimeter then as a Mm scatterometer. The MMA sample is an array of gold crosses whose crossbars alternate between 2.0 and 3.2-μm in length and are 400-nm wide, for an overall unit cell dimension of 7-μm, on a dielectric background. For comparison, an IR-VASE (J.A. Woollam, Co.) was used to take reflectance measurements. Figure 2 shows the results of the IR-VASE measurements and clearly shows a resonant feature at 5.0-μm and no resonant feature at 4.4-μm. Using one EC-QCL tuned

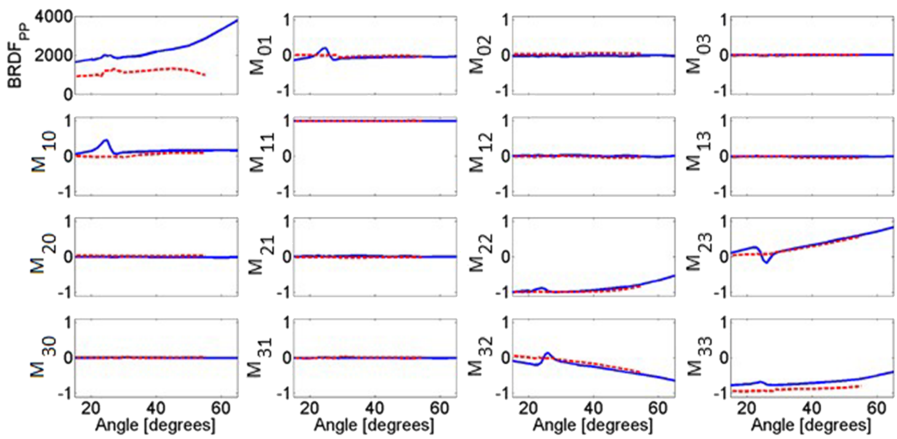

FIG. 3. Specular-reflectance Mm plot at 5.0-μm (solid blue line) and 4.4-μm (dashed red line) wavelengths for an IR MMA sample similar to that described in the work of Liu[16] when the instrument operates as a Mm polarimeter, i.e., in the specular mode such that the angle in each Mm element represents both incident and reflected angles. Note that the nanostructure's spectrally, directionally, and polarimetrically unique resonance at 5.0-μm is identified at 25° in several of the elements.

to 5.0-μm wavelength and another tuned to 4.4-μm, the impetus for building this instrument is clearly demonstrated, i.e., to investigate the polarimetric content of resonant and off-resonant narrowband features of IR nanostructured optical materials both at and away from specular angles.

A. Example spectral Mm polarimetric characterization

Our instrument was set to collect the specular reflectance from the IR metamaterial absorber over a solid angle of 50 μsr (i.e., 4-mm aperture diameter at a 50-cm distance) at incident angles ranging 15°-65°, with 1° increments collected over 20°-30° near the resonant condition of θ_i = 25°, and with 5° increments outside this region. This measurement was repeated twice to demonstrate the importance of spectral tunability. First, the wavelength was tuned to 5.0-μm which corresponds to a spectral resonant feature which was dependent on the incident angle of the source. The instrument was then tuned to 4.4-μm where there was no observed resonant feature.

Figure 3 shows the Mm results in the traditional 4×4 Mm format, but where each element is now a plot of the behavior of that element as a function of incident (and in this case, equivalently reflectance) angle. The plot in the m_{00} position

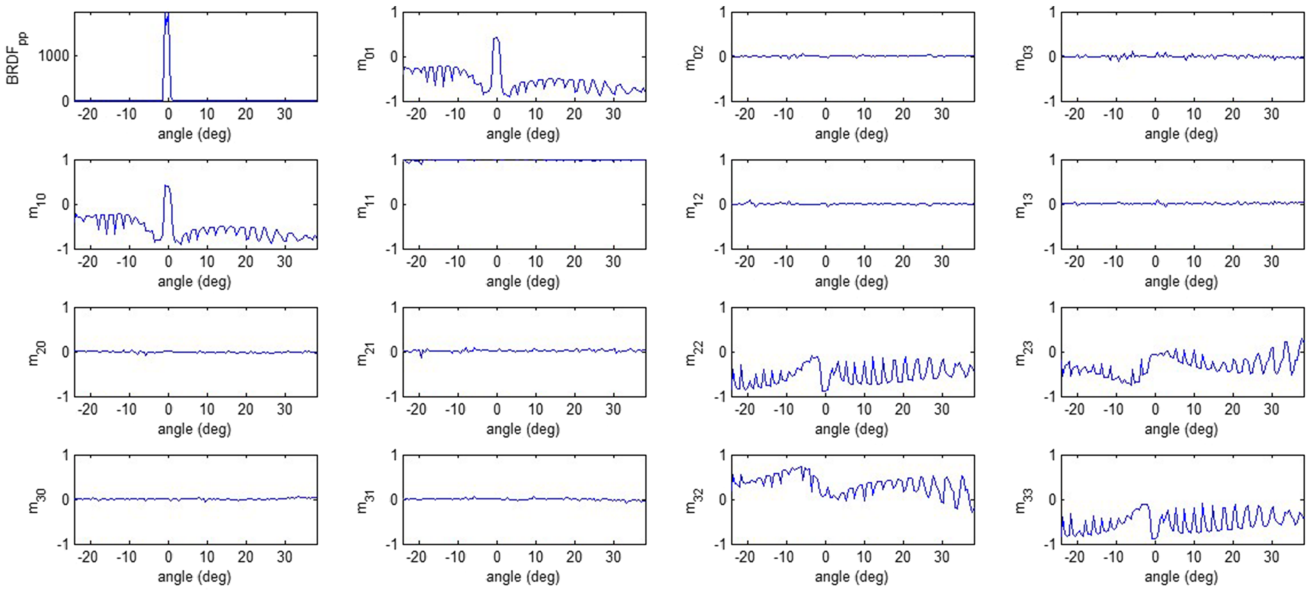

(a)

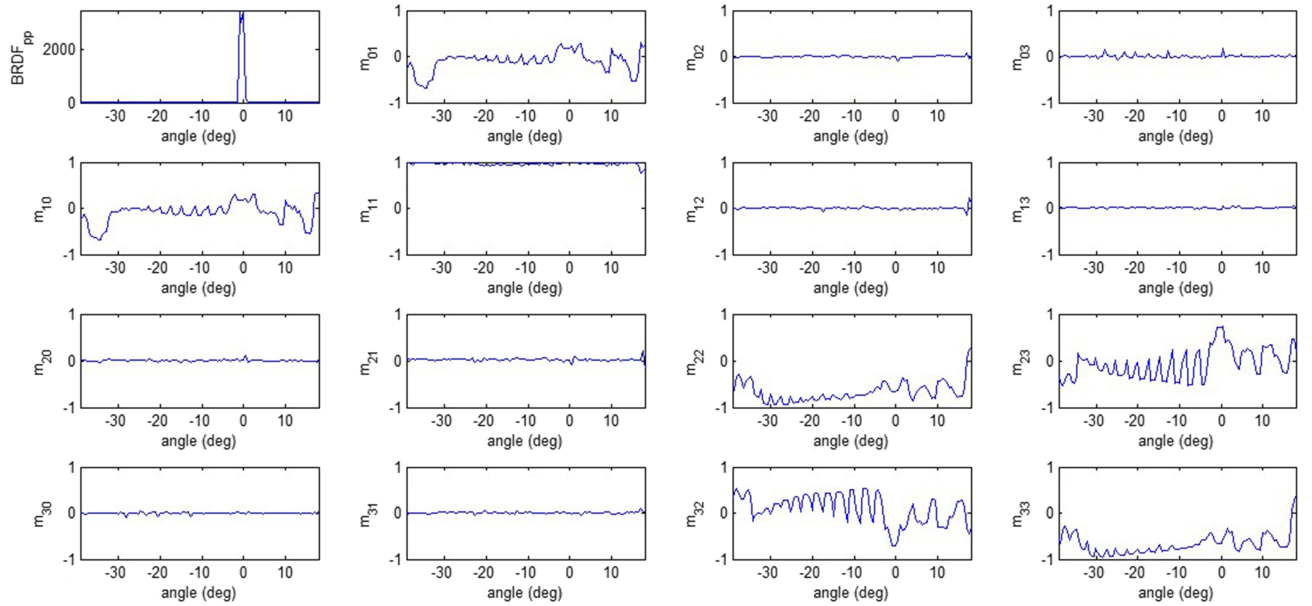

(b)

FIG. 4. Mm BRDF of an IR MMA sample similar to that described in the work of Liu[16] at 5.0-μm wavelength and (a) 25° and (b) 60° incident angles. In (a), the resonant feature shown in Fig. 2 is observed here at 0° (i.e., the specular angle). The Mm in (b) represents an off-resonance condition, and no unique features at specular (i.e., 0°) are observed. In both (a) and (b), the periodic structure observed is due to diffraction from a 140-μm EBL periodicity which was superimposed on the 7-μm IR unit cell periodicity during fabrication.

shows the first measurement collected at each incident angle, which is the co-polarization (i.e., p-polarization incident and p-polarization reflected) Bidirectional Reflectance Distribution Function (BRDF) value. In this case, the presence of the resonant feature in this IR metamaterial at $\theta_i = 25°$ is first observed in the m_{00} element at a wavelength of 5.0-μm (solid blue lines in Fig. 3). It is more clearly observed in several of the other Mm elements (m_{01}, m_{10}, m_{22}, m_{23}, m_{32}, and m_{33}) at the 5.0-μm wavelength and is clearly incident-angle dependent. Note that this feature is only accessible with the wavelength tunability and is not observable with the 4.4-μm measurement (dashed red lines).

Away from this resonant feature, the underlying Mm behavior indicates that this metamaterial acts like a metal mirror at these wavelengths. The resonance incident angle of 25° is believed to be the phase-matching condition for a Surface Plasmon Polariton (SPP) mode in this nanostructure. At resonance, this metamaterial displays both polarizer and retarder characteristics. The polarizer characteristics are observed in the m_{00}, m_{01}, and m_{10} elements and show that the reflectance of incident p-polarized light at the wavelength of 5.0-μm is reduced significantly at this incident angle. The retarder characteristics are observed in the m_{22}, m_{23}, m_{32}, and m_{33} elements and show that the phase of reflected s-polarized light at the 5.0-μm wavelength and 25° incidence angle lags than that of the reflected p-polarized light.

B. Example directional characterization

The same IR metamaterial was also examined with our instrument set as a Mm scatterometer. Figure 4 is again in the Mm format but now shows data collected at a wavelength of 5.0-μm and incident angles of (a) 25°, the observed resonant condition, and (b) 60°, an off-resonant angle. As a scatterometer, the instrument collects the Mm BRDF, so the angles shown for each Mueller element represent the in-plane reflectance angle for that particular incident angle. In Fig. 4(a) at the specular angle of 25° (represented by 0° in each Mm element), the same information shown in Fig. 3 at 25° is shown again here. Away from specular, diffraction orders are observed, indicating that this sample was fabricated in "tiles" approximately 140 μm in size [the mask size of this particular electron-beam lithography (EBL) process] and "tiled" together in a square lattice to form the larger sample. The polarization content of the light scattered by this sample is superimposed on this diffraction pattern. In Fig. 4(b), the information in Fig. 3 at 60° (where there is no resonant feature) is again shown at 0° (again, specular). Diffraction orders similar to those of Fig. 1(a) and the superposition of polarimetric information on these orders are again observed.

IV. CONCLUSION

Analyses of the spectral, directional, and polarimetric behaviors of narrowband resonant features observed in nanostructured optical materials have previously been constrained by the limited data available from broadband instruments such as spectrometers used primarily at specular angles in reflectance or transmittance and under limited polarimetric conditions. We have developed a tunable IR Mm polarimetric scatterometer to more fully explore the narrowband features of nanostructured optical materials, both at and away from specular and both in and out of the plane of incidence. A significant up-front analysis allowed this instrument to be designed and built in an optimal DRR polarimeter configuration, and the free-space results demonstrate the excellent calibration performance. The example measurements of an IR metamaterial selective absorber demonstrate this instrument's unique capability to provide novel spectral, directional, and polarimetric information on such samples.

ACKNOWLEDGMENTS

The authors wish to thank Mr. Tom Fitzgerald of the University of Dayton Research Institute for initial specifications on the instrument design and Professor W. Padilla of Duke University for providing the IR metamaterial sample. This research was supported by the Air Force Research Laboratory, Wright-Patterson AFB OH. The views expressed in this paper are those of the authors and do not necessarily reflect the official policy or position of the Air Force, the Department of Defense or the U.S. government.

[1]T. M. Fitzgerald and M. A. Marciniak, "Full optical scatter analysis for novel photonic and infrared meta-materials," Adv. Sci. Technol. **75**, 240–245 (2010).
[2]T. M. Fitzgerald, M. A. Marciniak, and S. E. Nauyoks, "Development of a tunable polarimetric scatterometry system in the MWIR and LWIR," Proc. SPIE **7792**, 779209 (2010).
[3]J. C. Vap, S. E. Nauyoks, T. M. Fitzgerald, and M. A. Marciniak, "Development of tunable polarimetric optical scattering instrument from 4.3-9.7 microns," Proc. SPIE **8154**, 81540E (2011).
[4]J. C. Vap, S. E. Nauyoks, and M. A. Marciniak, Meas. Sci. Technol. **24**, 055901 (2013).
[5]C. Menzel, C. Rockstuhl, T. Paul, and F. Lederer, Phys. Rev. B **77**, 195328 (2008).
[6]M. R. Benson, A. G. Kinsley, M. A. Marciniak, M. D. Seal, and A. M. Urbas, IEEE Photonics J. **7**, 2600613 (2015).
[7]C. R. Simovski and S. A. Tretyakov, Phys. Rev. B **75**, 195111 (2007).
[8]J. C. Vap and M. A. Marciniak, "Examining epsilon near zero structures through effective medium theory and optical thin-film analysis," Proc. SPIE **8364**, 8364–8426 (2012).
[9]M. M. Jakovljevic, G. Isic, B. Vasic, T. W. H. Oates, K. Hinrichs, I. Bergmair, K. Hingerl, and R. Gajic, "Spectroscopic ellipsometry of split ring resonators at infrared frequencies," Appl. Phys. Lett. **100**, 161105 (2012).
[10]M. A. Marciniak, S. R. Sellers, R. B. Lamott, and B. T. Cunningham, "Bidirectional scatter measurements of a guided mode resonant filter photonic crystal structure," Opt. Express **20**(25), 27242–27252 (2012).
[11]D. B. Burckel, J. R. Wendt, G. A. Ten Eyck, A. R. Ellis, I. Brener, and M. B. Sinclair, "Fabrication of 3D metamaterial resonators using self-aligned membrane projection lithography," Adv. Mater. **22**, 3171–3175 (2010).
[12]D. B. Burckel, J. R. Wendt, G. A. Ten Eyck, J. C. Ginn, A. R. Ellis, I. Brener, and M. B. Sinclair, "Micrometer-scale cubic unit cell 3D metamaterial layers," Adv. Mater. **22**, 5053–5057 (2010).
[13]B. Jia, S. Wu, J. Li, and M. Gu, "Near-infrared high refractive-index three-dimensional inverse woodpile photonic crystals generated by a sol-gel process," J. Appl. Phys. **102**(9), 096102 (2007).
[14]C. Wu, B. Neuner III, J. John, A. Milder, B. Zollars, S. Savoy, and G. Shvets, "Metamaterial-based integrated plasmonic absorber/emitter for solar thermo-photovoltaic systems," J. Opt. **14**(2), 024005 (2012).
[15]I. El-Kady, R. Biswas, Y. Ye, M. F. Su, I. Puscasu, M. Pralle, E. A. Johnson, J. Daly, and A. Greenwald, "Tunable narrow-band infrared emitters from hexagonal lattices," Photonics Nanostruct. Fundam. Appl. **1**, 69–77 (2003).
[16]X. Liu, T. Tyler, T. Starr, A. F. Starr, N. M. Jokerst, and W. J. Padilla, "Taming the blackbody with infrared metamaterials as selective thermal emitters," Phys. Rev. Lett. **107**, 045901 (2011).

[17]H. Sai, H. Yugami, Y. Kanamori, and K. Hane, "Spectrally selective thermal radiators and absorbers with periodic microstructured surface for high-temperature applications," Microscale Thermophys. Eng. **7**, 101–115 (2003).
[18]N. Dahan, A. Niv, G. Biener, Y. Gorodetski, V. Kleiner, and E. Hasman, "Enhanced coherency of thermal emission: Beyond the limitation imposed by delocalized surface waves," Phys. Rev. B **76**, 045427 (2007).
[19]N. Dahan, A. Niv, G. Biener, Y. Gorodetski, V. Kleiner, and E. Hasman, "Extraordinary coherent thermal emission from SiC due to coupled resonant cavities," J. Heat Transfer **130**, 112401 (2008).
[20]S. Y. Lin, J. Moreno, and J. G. Fleming, "Three-dimensional photonic-crystal emitter for thermal photovoltaic power generation," Appl. Phys. Lett. **83**(2), 380–382 (2003).
[21]T. S. Luk, T. Mclellan, G. Subramania, J. C. Verley, and I. El-Kady, "Emissivity measurements of 3D photonic crystals at high temperatures," Photonics Nanostruct. Fundam. Appl. **6**, 81–86 (2008).
[22]F. Marquier, K. Joulain, J.-P. Mulet, R. Carminati, J.-J. Greffet, and Y. Chen, "Coherent spontaneous emission of light by thermal sources," Phys. Rev. B **69**, 155412 (2004).
[23]H. Sai, H. Yugami, Y. Akiyama, Y. Kanamori, and K. Hane, "Spectral control of thermal emission by periodic microstructured surfaces in the near-infrared region," J. Opt. Soc. Am. A **18**(7), 1471–1476 (2001).
[24]Y. X. Yeng, M. Ghebrebrhan, P. Bermel, W. R. Chan, J. D. Joannopoulos, M. Soljačić, and I. Celanovic, "Enabling high-temperature nanophotonics for energy applications," Proc. Natl. Acad. Sci. U. S. A. **109**(7), 2280–2285 (2012).
[25]F. Kusunoki, T. Kohama, T. Hiroshima, S. Fukumoto, J. Takahara, and T. Kobayashi, "Narrow-band thermal radiation with low directivity by resonant modes inside tungsten microcavities," Jpn. J. Appl. Phys., Part 1 **43**(8A), 5253–5258 (2004).
[26]J.-H. Lee, J. C. W. Lee, W. Leung, M. Li, K. Constant, C. T. Chan, and K.-M. Ho, "Polarization engineering of thermal radiation using metallic photonic crystals," Adv. Mater. **20**, 3244–3247 (2008).
[27]J. Le Gall, M. Olivier, and J.-J. Greffet, "Experimental and theoretical study of reflection and coherent thermal emission by a SiC grating supporting a surface-phonon polariton," Phys. Rev. B **55**(15), 10105–10114 (1997).
[28]F. O'Sullivan, I. Celanovic, N. Jovanovic, J. Kassakian, S. Akiyama, and K. Wada, "Optical characteristics of one-dimensional Si/SiO_2 photonic crystals for thermophotovoltaic applications," J. Appl. Phys. **97**(3), 033529 (2005).
[29]P. J. Hesketh, J. N. Zemel, and B. Gebhart, "Polarized spectral emittance from periodic micromachined surfaces. I. Doped silicon: The normal direction," Phys. Rev. B **37**(18), 10795–10802 (1988).
[30]P. J. Hesketh, J. N. Zemel, and B. Gebhart, "Polarized spectral emittance from periodic micromachined surfaces. II. Doped silicon: Angular variation," Phys. Rev. B **37**(18), 10803–10813 (1988).
[31]J. Zhu, Z. Yu, S. Fan, and Y. Cui, "Nanostructured photon management for high performance solar cells," Mater. Sci. Eng., R **70**, 330–340 (2010).
[32]M. Benson, P. Shah, M. Marciniak, A. Sarangan, and A. Urbas, "Optical characterization of silver nanorod thin films grown using oblique angle deposition," J. Nanomater. **2014**, 694982.
[33]D. B. Chenault, J. L. Pezaniti, and R. A. Chipman, "Mueller matrix algorithms," Proc. SPIE **1726**, 231–246 (1992).
[34]R. M. A. Azzam, "Photopolarimetric measurement of the Mueller matrix by Fourier analysis of a single detected signal," Opt. Lett. **2**(6), 148–150 (1978).
[35]D. S. Sabatke, M. R. Descour, E. L. Dereniak, W. C. Sweatt, S. A. Kemme, and G. S. Phipps, "Optimization of retardance for a complete Stokes polarimeter," Opt. Lett. **25**(11), 802–804 (2000).
[36]M. Smith, "Optimization of a dual-rotating retarder Mueller matrix polarimeter," Appl. Opt. **41**(13), 2488–2493 (2002).
[37]D. Goldstein, *Polarized Light* (CRC Press, Boca Raton, FL, 2003).